UHASSELT
KNOWLEDGE IN ACTION

Maastricht University

Faculty of Medicine and Life Sciences
School for Life Sciences
Master of Biomedical Sciences

Master's thesis

Development of an in vitro model for drug screening in Alzheimer's Disease

Nida Ünal

Thesis presented in fulfillment of the requirements for the degree of Master of Biomedical Sciences, specialization Molecular Mechanisms in Health and Disease

SUPERVISOR :
Prof. dr. Ilse DEWACHTER

SUPERVISOR :
dr. Yanick FANTON

MENTOR :
Teun VAN NUNEN
dr. Jolien BEEKEN

2021
2022

Transnational University Limburg is a unique collaboration of two universities in two countries: the University of Hasselt and Maastricht University.

UHASSELT
KNOWLEDGE IN ACTION

www.uhasselt.be
Universiteit Hasselt
Campus Hasselt:
Martelarenlaan 42 | 3500 Hasselt
Campus Diepenbeek:
Agoralaan Gebouw D | 3590 Diepenbeek

Maastricht University

Faculty of Medicine and Life Sciences
School for Life Sciences
Master of Biomedical Sciences

Master's thesis

Development of an *in vitro* model for drug screening in Alzheimer's Disease

Nida Ünal

Thesis presented in fulfillment of the requirements for the degree of Master of Biomedical Sciences, specialization Molecular Mechanisms in Health and Disease

SUPERVISOR :
Prof. dr. Ilse DEWACHTER

SUPERVISOR :
dr. Yanick FANTON

MENTOR :
Teun VAN NUNEN
dr. Jolien BEEKEN

Development of an *in vitro* model for drug screening in Alzheimer's Disease.

Nida Ünal[1], Teun van Nunen[2], Jolien Beeken[2] and Yanick Fanton[2]

[1]Universiteit Hasselt, Campus Diepenbeek, Agoralaan Building C - 3590 Diepenbeek, Belgium
[2]InnoSer Laboratories Belgium NV, BioVille, Agoralaan Building Abis - 3590 Diepenbeek, Belgium

*Running title: *Optimization of an in vitro model for AD (< 50 characters inc. spaces, italic)*

To whom correspondence should be addressed: Yanick Fanton, Tel: +32 472 55 02 96; Email: YFanton@innoserlaboratories.com

Keywords: Alzheimer's, spheroids, SH-SY5Y, Tau, okadaic acid, *in vitro*

ABSTRACT

Alzheimer's Disease (AD) drug development is being held back by the lack of suitable research models. Animal models have limited translatability and 2D cellular models lack the complexity of the human brain. However, better cellular models are increasingly being studied. Using the neuroblastoma SH-SY5Y cell line, we aim to develop an *in vitro* AD model to test novel therapeutic compounds targeting the neurofibrillary tangles in AD. As a first step in a multi-step platform, this cell line will overcome the high costs and duration accompanied by human stem cell derived cellular models, whereas still allowing to assess several specific disease processes in a cost-efficient human model. Hereby, this study explored the induction of Tau hyperphosphorylation via okadaic acid induction in SH-SY5Y cells. Additionally, growing these cells into a 3D model will provide better determination of intercellular connectivity, consequently creating a more translational model showing mis-localization and higher levels of phosphorylated Tau.

Okadaic acid treated SH-SY5Y cells remained viable at concentrations up to 10 nM and hyperphosphorylated Tau was obtained starting from the same concentration. Ca^{2+}-imaging was performed to assess neuronal activity and an initial ROS induction was performed to make a shift towards the Aβ-pathology incorporated in our model.

This SH-SY5Y model will serve as a cheaper and faster model before moving to more complex stem cell-derived *in vitro* models carrying specific mutations and *in vivo* models. This way, our model will be the first step in a multi-step drug-screening platform.

INTRODUCTION

Neurodegenerative disorders such as Alzheimer's disease (AD) or Parkinson's disease (PD) are one of the main threats to human health, considering both death and disability worldwide (1). Amongst affecting millions of people globally, both physically and mentally, they are also accompanied by a high economic burden (2). More specifically, Alzheimer's Disease (AD), the most prominent type of dementia, is the leading neurodegenerative disorder worldwide. This cerebral disorder involves progressive loss of cognitive functions, memory loss and spatial disorientation (3). Besides age being the most prominent risk factor, genetics and environmental factors, like head injuries and exposure to pollution and pesticides, contribute to the development and progression of this disorder (4). Due to the aging global population and their increasing longevity combined with increasing industrialization, the prevalence rate of AD is expected to double within the coming 20 years (5). The vast majority of AD cases are sporadic, with the onset usually starting around the age of 65 (6). However, rare familial forms of AD (<0.5%) exist that are caused by specific genetic mutations in the amyloid precursor protein (APP), in presenilin 1 (PSEN1), or presenilin 2 (PSEN2). These rare forms of AD develop earlier around the age of 30 to 50 (7, 8).

The pathophysiology behind AD primarily consists of the accumulation of intracellular neurofibrillary tangles (NFTs) inside the neuron and the formation of extracellular amyloid beta (Aβ) plaques (9). The NFTs consist of the aggregated and accumulated hyperphosphorylated microtubule-associated protein (MAP) Tau (10). In normal physiological conditions, human protein Tau is found in a highly soluble and unfolded state, where it interacts with

tubulin to promote the assembly of microtubules. Hereby, Tau stabilizes the dynamic structures of the cytoskeleton hence generating cytoplasmic extensions in specific directions. These cytoplasmic extensions evolve in axons and dendrites that are important for electrochemical signaling inside the brain (11).

Upon AD pathological conditions, the phosphorylation rate of Tau is significantly higher, carrying nine phosphates per molecule in comparison to two or three phosphate residues in physiological conditions (3). Hyperphosphorylation of Tau is followed by oligomerisation in which Tau fibrillates and aggregates into NFTs, leading to abnormal neuronal functions and neuronal loss (9).

The formation of extracellular senile plaques on the other hand consists of accumulated Aβ peptide depositions. The Aβ peptide is a 4 kDa fragment of the amyloid precursor protein (APP). Under normal conditions APP is cleaved by α-secretase and then by ɣ-secretase. However, under pathological conditions APP is instead cleaved by β-secretase before ɣ-secretase, resulting in Aβ42 carrying 2 additional hydrophobic C-terminal residues in comparison to the normal Aβ40. The Aβ42 is insoluble, proceeding in its aggregation and fibrillization, this way forming the core of neurotic senile plaques in the AD brain (12, 13). It has been described that reactive oxygen species (ROS) are implicated in Aβ-induced neurotoxicity as oxidative agents are described to increase Aβ production (14, 15). More interestingly, the proteolytic function of ɣ-secretase is regulated by presenilin 1 (PSEN1) and presenilin 2 (PSEN2). Mutations in these proteins will change the activity of ɣ-secretase and increase the ratio of Aβ in early-onset forms of AD (16, 17).

Current therapies are focused on the alleviation of symptoms in AD patients (18). Unfortunately, many disease-modifying drugs for AD fail in clinical trials, leading to an increasing gap in drug development. Recent research focused on treatment of both cognitive disturbance and behavioural symptoms, however, a cure that reverses the pathophysiology of AD remains elusive (19). Moreover, the heterogenous aetiology behind the pathological hallmarks contributes to the urgent need for optimal therapies (20). In addition to an inadequate understanding of the biology behind AD, limitations in experimental models contribute to this failure rate (21).

It is important to understand the efficient roles of the different research models. Initially, analyses in relevant *in vitro* models created from simple cell lines are desired before moving to more complex cellular models, e.g. 3D *in vitro* models. Afterwards, moving to distinguished *in vivo* models will contribute to obtaining relevant results. This way, a cost-efficient way of both drug development as drug screening will be guaranteed. All models have their own advantages and obstacles. Predominantly, *in vivo* models are being used to gain a better understanding of the pathogenesis and to screen the potential of novel therapeutic compounds. While studies in rats and mice have led to key insights in AD pathophysiology, these animal models are accompanied by limitations as no single model completely reproduces the pathophysiology occurring in patients. Notably, high failure rates of AD drugs in clinical trials, which were successful in preclinical *in vivo* models, raised questions about the translational value of these animal models. Frequently used *in vivo* models are transgenic mice, overexpressing human genes associated with familial AD. Other animals like *Drosophila melanogaster* and zebrafish are also potentially suited *in vivo* models, but given low conservation to human physiology they are less extensively used (22). Unfortunately, no existing animal model reflects the entire biological or pathological processes. On top of that, the slow onset of AD and the differences between humans and mice contribute to the lack of translatability (23). Therefore, results found in animal models will likely not accurately recapitulate the expected results in patients. Furthermore, these *in vivo* models are slow, complex, low throughput, costly and lead to increasingly intense ethical debates (24).

On the other hand, 2D *in vitro* models exist. Even though these simple cell models are low cost and low maintenance options, they consist of single-cell cultures and are not fully able to reproduce the spatial and temporal signaling present in the body (25). Hence, there is a pressing demand for breakthroughs in drug development, especially considering the expected rise in people affected by AD. As a result, the development of an innovative

human *in vitro* cellular model aims to overcome these limitations.
Recently, the development of 3D models to study several disorders gained lots of interest, providing new insights into human development, as well as therapeutic approaches on a platform more physiologically relevant (26). One of the most popular fields of studies in 3D *in vitro* models are organoids, which can be derived from human stem cells and are able to self-assemble into 3D structures in an *in vivo*-like manner (27). However, the development of this innovative bridging model between animal models and humans is not yet advanced. Key limiting factors in using organoids for drug screening are poor validation, poor standardization and their high cost (27). Therefore, the optimization of 2D *in vitro* models before moving to its 3D generation is important. Creating a representable cellular model is the first step before moving to more complex models, which will serve as a *in vivo*-like control.

Overall, research on neurodegenerative disorders like AD and PD, is hampered by the lack of suitable *in vitro* models to study the human neurobiology. Since human neurons are not readily available, various immortalized cell lines which can be differentiated into neuron-like cells are used in research. The SH-SY5Y is a widely used cell line with such characteristics (28). SH-SY5Y cells are originally derived from a metastatic bone marrow tumour biopsy of a neuroblastoma patient. The SH-SY5Y cell line is capable of large-scale expansion and relatively easy and cheap to culture compared to primary neurons or iPSC-derived neurons. Additionally, less ethical concerns are involved compared to the latter two cell types. On top of that, SH-SY5Y cells contain two morphologically distinct phenotypes; the neuroblast-like "N" phenotype and the epithelial-like "S" phenotype.

However, these cells lack precise features that define neurons, including neuronal morphology, inhibited cell division and expression of neuron-specific markers in undifferentiated state. Nevertheless, various methods to differentiate SH-SY5Y cells into neuron-like cells, exhibiting neuronal features such as axonal- and dendritic outgrowths, formation of functional synapses and network formation, are described in literature (29, 30). More interestingly, differentiated SH-SY5Y cells express forms of Tau with neuronal localization, making this cell line useful in neuroscience, particularly AD research (28).
In this manuscript, we describe the differentiation of SH-SY5Y cells into mature neuron-like cells. These cells will be treated with okadaic acid (OA) to induce Tau hyperphosphorylation occurring in AD. OA is a selective inhibitor of protein phosphatase 2A (PP2A), which is an important regulator of the phosphorylation state of microtubule-associated proteins that regulate assembly and stability of microtubule (31). Moreover, ROS will be induced by the means of hydrogen peroxide treatment in this *in vitro* model, to test its compliance before moving to inducing the Aβ pathology of AD. The neuronal activity of the achieved neuron-like cell model will be assessed by calcium imaging. Lastly, moving towards a 3D model with these SH-SY5Y cells will be initiated.

Compound-screening is a multi-step process considering both simple cellular models to complex cellular models and *in vivo* models. This manuscript focuses on acquiring AD-related pathological hallmarks in a simple cellular model and suggests the first step of a broader in-house project. As the previously described SH-SY5Y human neuroblastoma cells allow a quick and cost-efficient way of screening AD characteristics, this cell line will be used to run experiments in parallel to the experiments of the MINDMAP consortium considering Tau-specific mutated neuronal progenitor cells (NPCs). The SH-SY5Y cells will be used to perform all experiments and overcome the expensive and time consuming induced pluripotent stem cell-derived NPCs. This way creating a multi-step platform, in which the SH-SY5Y model will be a first step.

EXPERIMENTAL PROCEDURES

Cell culture

SH-SY5Y cells (gifted from the TU Eindhoven, the Netherlands) were grown in Dulbecco's modified Eagle medium (DMEM, Gibco Cat. No. 41966029, Paisley, Scotland) supplemented with 10% fetal bovine serum (FBS, heat inactivated, Thermo Fisher Scientific Cat. No. 10438026, Paisley, Scotland) and 1% Penicillin/Streptomycin (1% P/S, Thermo Fisher Scientific Cat. No. 15070063) in 37 °C, humidified air with 5% CO_2. Undifferentiated cells were grown to 90% confluency and seeded in

well plates at a density of 10.000 cells/cm^2 for further experiments. To start neuron-like differentiation, medium was changed the following day into DMEM (Gibco Cat. No. 41966039) containing 10 µM retinoic acid [RA (Sigma Aldrich, Cat. No. R2625)]. This medium was maintained for 2 days. At day 3, medium was replaced with differentiation medium two (DF2) consisting of Neurobasal-A minus phenol red medium (Gibco Cat. No. 12349015) containing 2 mM L-Glutamine (Gibco Cat. No. 25030024), 1x N-2 supplement (Gibco Cat. No. 17502048), 50 ng/mL human brain-derived neurotrophic factor (BDNF, Invitrogen Cat. No. RP-8642) and 1% P/S. Cells were left in DF2 until 7 days *in vitro* (DIV) for further experiments. Medium composition given in **supplementary table 2**.

Live cell imaging

To follow up the morphology of the cells, visualization with brightfield imaging was performed using a Leica microscope (DM IL LED Ser. No. 382007, Leica Microsystems CMS GmbH, Wetzlar, Germany). Cells were maintained in culture flasks and in 96-well plates (Greiner bio one, Cat. No. 655180), humidified at 37°C in 5% CO_2.

Immunofluorescence analysis

SH-SY5Y cells cultured on 96-well polystyrene plates were fixed with fixation buffer (4% paraformaldehyde in milli-Q) for 15 min at room temperature (RT), washed with washing buffer (0.2% Triton X-100 in PBS) and incubated with blocking buffer (PBS-T + 5% horse serum) for 1 h at RT. Afterwards, cells were incubated with primary antibodies (**Supplementary table 1**) overnight at 4°C, washed with washing buffer and incubated with. secondary antibody and NucBlue DAPI for 1 h at RT. Finally, cells were washed with washing buffer and left in PBS prior to imaging. Staining controls for the secondary antibodies were performed by omitting the primary antibodies. Images were acquired using the ImageXpress Micro 4 High Content imaging system (Molecular Devices, LLC. San Jose, CA, USA) and processed using the imagers build-in software or ImageJ (ImageJ 1.53C, U.S. National Institutes of Health, Marlyand, USA).

Cell viability

Cells were treated with increasing concentrations of OA (0 nM, 10 nM, 20 nM, 30 nM, 40 nM, 50 nM). After 24 h, viability was assessed using the quantitative colorimetric MTT assay kit (Cell Proliferation Kit I, Merck, Sigma-Aldrich Cat. No. 11465007001) following the manufacturer's instructions. Briefly, the MTT labeling reagent was added to each well at a final concentration of 0.5 mg/mL and incubated at 37°C with 5% CO_2 for 2 h. Metabolically active cells convert the yellow MTT tetrazolium compound into a purple formazan product. The insoluble formazan crystals were dissolved with the kits solubilization buffer. MTT reduction was assessed colorimetrical by measurement at 570 nm. Percentages of viability were calculated by comparison to untreated cells.

Calcium imaging

Calcium imaging was performed based on the Fluo-4 Calcium Imaging Kit protocol (Molecular Probes™, Thermo Fisher Scientific, Cat. No. F10489). Briefly, loading solution (100x Powerload™ concentrate, Fluo-4 AM 100x, 20 mM glucose stock in Live Cell Imaging Solution (LCIS) and 100x Probenecid) were administered to the cells and left incubating for 1 h at 37 °C followed by washing with LCIS and incubation with imaging solution (20 mM glucose stock in LCIS and 10% Neuro Backdrop Background Suppressor solution). Hereafter, cells were imaged during a time series (5 s interval) before and/or after being exposed to 10 µM Ionomycin (Thermo Fisher Scientific, Cat. No. I24222) using the Molecular Devices' imager and MetaXpress high-content image acquisition and analysis software. A timelapse video was generated to give a visual representation of calcium flux of the cells in the focal plane.

Measurement of Intracellular ROS

Intracellular ROS was measured using the DCFDA / H2DCFDA kit (Cellular ROS Assay kit, Abcam Cat. No. ab113851, Cambridge, UK) according to the manufacturer's instructions. SH-SY5Y cells were seeded into 96-well plates at a density of 25.000 cells/well. Cells were treated with ascorbic acid (AA) for 4 h, then washed with 1x buffer provided in the kit, stained with 10 µM DCFDA for 45 min at 37 °C protected from light, washed again followed by incubation with concentrations AA (0 µM, 10 µM, 20 µM, 40 µM, 60 µM and 100 µM) +

H_2O_2 (600 µM and 800 µM) at 37 °C in a humidified incubator with 5% CO_2. Additionally, experiments with concentrations compound x (40 µM and 80 µM) instead of AA were performed following the same protocol. Measurements were performed after different time periods (15 min, 30 min, 1 h, 2 h, 3 h, 4 h, 5 h and 6 h) using the Glomax Discovery plate reader (Promega Corporation, Madison, USA) at excitation/emission wavelengths of 485/535 nm, respectively. The value of fluorescence intensity was obtained by the ratio of fluorescent intensity at a specific timepoint over fluorescent intensity at time 0 (baseline), which was measured prior to exposure and immediate after staining with DCFDA.

3D Spheroid generation

SH-SY5Y cells were seeded in Aggrewell800™ (STEMCELL Technologies, Cat. No. 34811) at a density of 3 x 10^6 cells per well according to the manufacturer's instructions. Before seeding, the wells were coated with anti-adherence solution (500 µL/well) and the plate was centrifuged at 1300 g for 5 min. Wells were washed with 2 mL medium and cells were seeded in 1 mL. The plate was centrifuged at 100 g for 3 min to ensure trapping of the cells in the pockets. Lastly, spheroids were replated to ultra-low attachment plates (Corning, Cat. No. 10717009, Kennebunk, USA) to ensure that spheroids will keep their form and clustering structure.

Statistical Analysis

Analysis was performed with GraphPad Prism 9.3.1 (GraphPad Software, San Diego, California USA). Results were presented as mean values ± SEM.

For statistical comparisons, data distribution was assessed for normality (Shapiro-Wilk test). In case these assumptions were met for all groups, quantitative data was analyzed by one-way analysis of variance (ANOVA). In case normality was not met a non-parametric test (Kruskal-Wallis) was used. P-values smaller than 0.05 were considered significant.

RESULTS

SH-SY5Y cells achieve neuronal morphological characteristics

Prior to commencing the experiments, it was important to determine the culturing conditions in which SH-SY5Y neuroblastoma cells reduce in cell body size and develop neuronal projections that are important to connect with surrounding cells hereby mimicking the shape of human neuronal cells. To achieve this, SH-SY5Y cells were cultured in differentiation media with RA, BDNF and serum starvation. To demonstrate that SH-SY5Y cells can be differentiated to a neuronal-like phenotype, cell morphology changes were examined. While undifferentiated SH-SY5Y neuroblastoma cells show an epithelial-like phenotype (**Fig. 1 A**), cells cultured in differentiation medium 1 and 2 (DF1 + DF2) with RA and BDNF displayed clear neurite branching as seen in neurons (**Fig. 1**). In addition, differentiating SH-SY5Y cells were examined at different days after the start of differentiation showing gradual changes towards a neuron-like morphology based on neurite outgrowth quantification. **Figure 1, B** represents SH-SY5Y neuroblastoma cells still showing epithelial like morphologies at 1DIV. The shift to a more significant neuronal phenotype happens at around 7DIV (**Fig. 1 C**). By morphological assessment, cell differentiation seems to be optimal at 14DIV, where cell bodies and neurites seem most alike true human neuronal cells. Moreover, the morphology of the cells at 21DIV revert to the typical epithelial-like cell bodies (**Fig. 1 E**). On top of this, strong cluster formation is observed throughout the culture, resulting in less observable neurite outgrowth.

More specifically, neurite branching was quantitatively assessed for all different timing points (0DIV, 1DIV, 7DIV, 14DIV and 21DIV). Quantification confirmed 14DIV differentiation results in optimal neuronal morphology.

Immunofluorescence staining for neuron-specific markers indicate achievement of neuronal characteristics of differentiated SH-SY5Y cells

It is important to validate that the SH-SY5Y cells have obtained a neuronal-like phenotype, rather than accepting this by visual observations. For that reason, immunofluorescence staining for different neuronal markers was performed. To confirm differentiation is most optimal at 14DIV, cells at 21DIV were also taken into the experiment. During differentiation and the formation of networks, the migration of SH-SY5Y cells was observed, therefore cells are not evenly distributed, resulting in areas with various densities across the culture. For the particular analysis, fluorescent images of areas containing less dense networks of cells were used. Neurites in these areas are more clearly visible, making it easier to distinguish and properly image them, as well as spotting small structures such as synapses.

First, staining of differentiated SH-SY5Y cells was assessed to investigate; microtubule-associated protein 2 (MAP2) and nuclear staining DAPI. Both differentiated SH-SY5Y cells at 14DIV and 21DIV stain positive for mature neuronal marker MAP2, although less branching, loss in intercellular connections, is observed at 21DIV (**Fig. 2 A**). Further analysis was performed in 14DIV cells. Differentiated cells stained positive for neurofilament200 (NF200). Mature neurons exhibit information transport via synaptic connections. Therefore, synapse analysis using double staining for synaptophysin (SYN) and postsynaptic density protein 95 (PSD95) was performed. While SYN is a presynaptic marker, PSD95 is a postsynaptic adaptor on the excitatory postsynapses. As a result, signals that are double-positive for both markers, are synapses and validate the neuronal phenotype. Cells are differentiated with RA and BDNF on top of serum starvation. High cell viability and the clear presence of neuronal markers show successful differentiation using the method described (**Fig. 2 B)**.

Okadaic acid reduces cell viability of SH-SY5Y cells.

To determine the cytotoxic effect of OA on the generated cell model, differentiated SH-SY5Y cells were incubated with increasing concentrations of okadaic acid (OA) for 24 h and cell viability was examined by the MTT assay. Treatment of OA at 20, 30, 40 and 50 nM decreased the viability of SH-SY5Y cells to 20%, 6%, 17% and 8% respectively (**Fig. 3**).

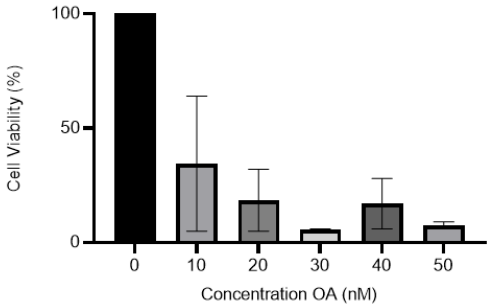

Figure 3 – Effects of OA-induced cytotoxicity in SH-SY5Y cells. SH-SY5Y cells were treated with different concentrations of OA as 10, 20, 30, 40 and 50 nM for 24h. Bar graph is presented as the percentage of control (0 nM OA) MTT value. Data are expressed as mean ± SEM.

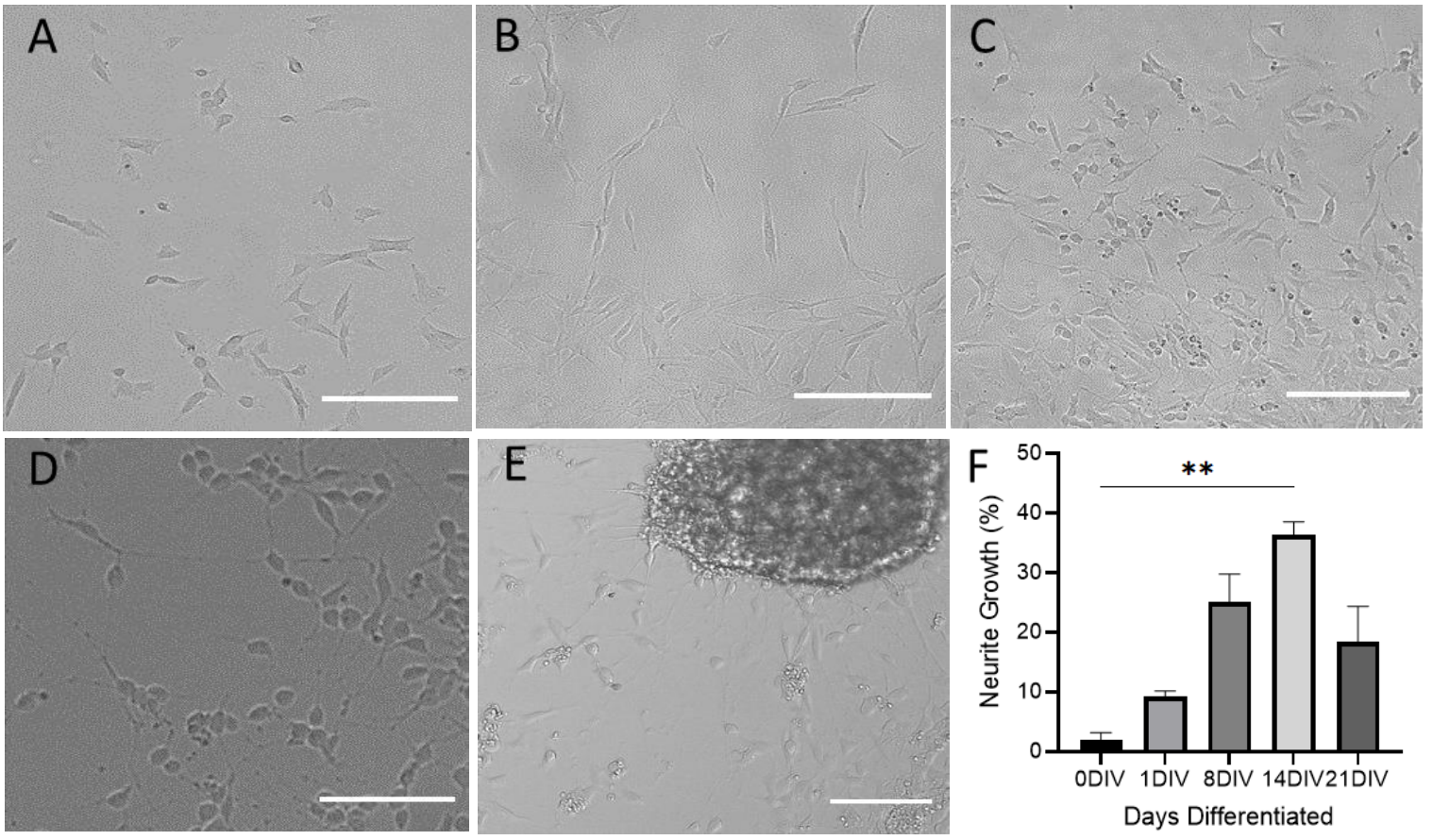

Figure 1 – Representative images (A-E) of SH-SY5Y cells showing neurite growth after differentiation. A) 0DIV; epithelial-like cell bodies, no neuronal branching. **B)** 1DIV (in DF1); morphologic alterations, novice neurite branching, grouping of cells **C)** 7DIV (in DF2); rounder soma, clear neuronal-like morphology, visible neurite branching (both short as long branching), clusters of cells grouped together and connected with branches that resemble a neuronal culture. **D)** 14DIV (in DF2); notable ideal stellate morphology and abundance of neurites **E)** 21DIV (in DF2); more extensive network formation, dedifferentiation, longer epithelial-like cell bodies. All pictures are made with a 10x objective. Scale bar 28 µm. **F)** Neurite growth was quantified by counting the number of cells showing neurites that were twice of the cell body diameter in length. The proportion of cells with neurites was expressed as a percentage of the total number of cells. Data are expressed as mean ± SEM (n=3), n too small to assess normality. Kruskal-Wallis test, *$\alpha = 0.05$, ** $p = 0.0047$.*

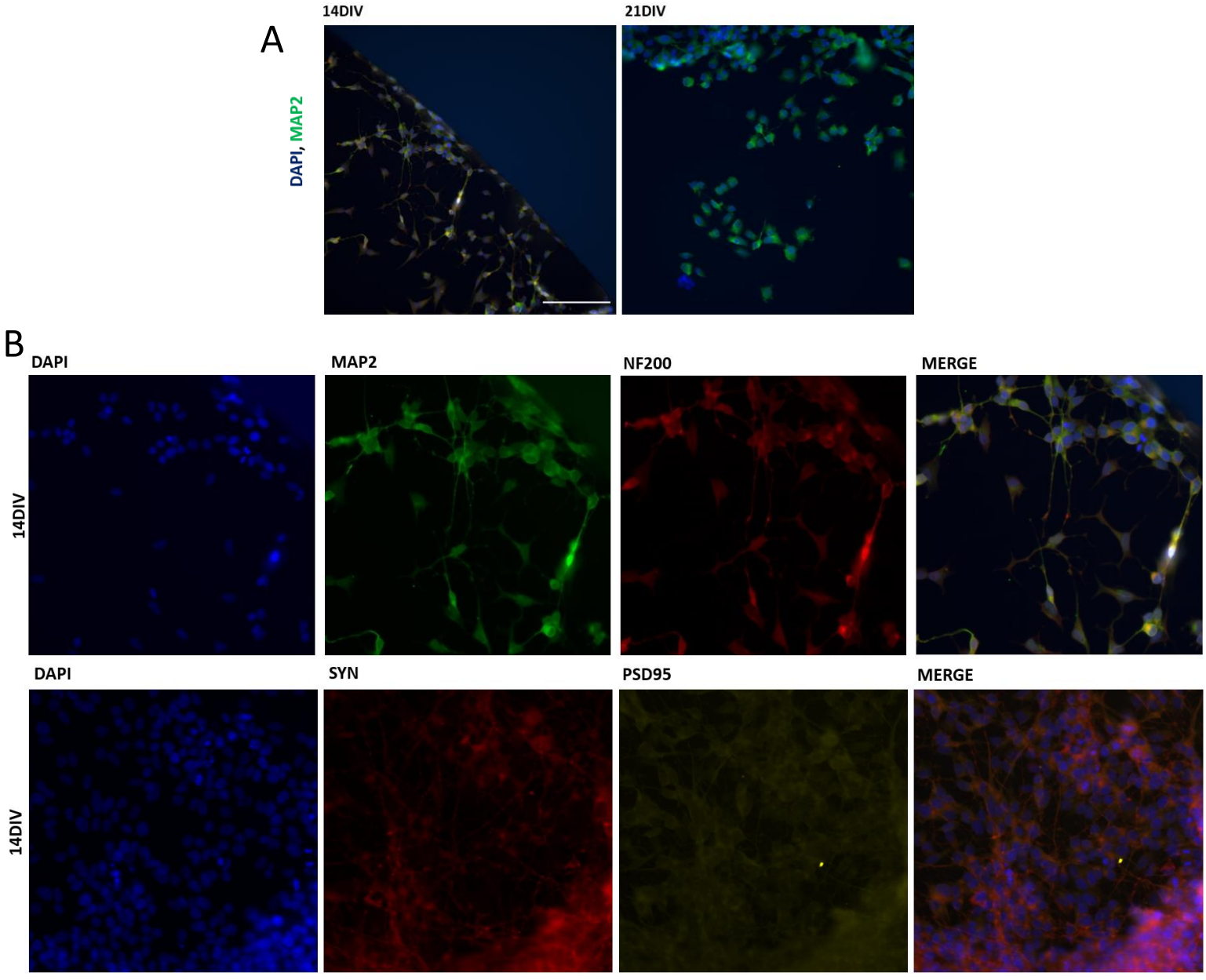

Figure 2 – **Immunofluorescence staining for neuronal markers of differentiated SH-SY5Y cells. A)** MAP2 staining, the comparison was made between SH-SY5Y cells at 14DIV and 21DIV to determine optimal differentiation duration. **B)** Staining of neuronal markers at 14DIV. Pictures were made at 20x magnification, cells were seeded at 3000 cells/well. Scalebar 162,5 µm.

Okadaic acid induction leads to Tau hyperphosphorylation, mis-localization, and neuronal cell death.

To establish standardized screening assays using an *in vitro* SH-SY5Y cell model it is essential to demonstrate an AD-like Tau pathology. To achieve this, we induced Tau pathological hyperphosphorylation by incubating the cells with okadaic acid (OA) in a concentration range (0 nM, 10 nM, 20 nM, 30 nM, 40 nM and 50 nM).

A quantitative analysis of fluorescence intensity of phosphorylated-tau (referred to as pTau) was performed after incubation with different concentrations of OA on 14DIV SH-SY5Y cells. Based on the obtained results, 20 nM was determined as the optimal concentration to induce visible Tau hyperphosphorylation (**Fig. 4**). Corrected total cell fluorescence values of OA-acid treated 14DIV SH-SY5Y cells are given in **fig. 5**. However, these cells showed less to no branching (**Supplementary Fig. 1**). Remarkably, OA treatment might be too strong for the less densely differentiated 14DIV cells. Immunofluorescence analysis was also performed on 19DIV SH-SY5Y cells (**Fig. 5)**, this time dense structures containing neuronal branching were still preserved and pTau mis-localization was observable.

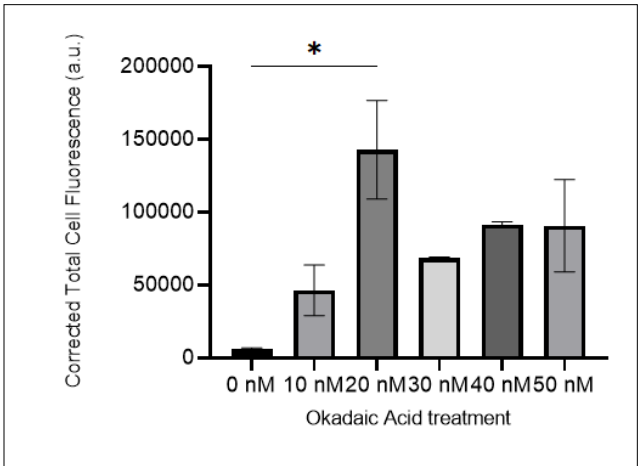

Figure 4 – Corrected Total Cell Fluorescence (CTCF) for OA-treated 14DIV SH-SY5Y cells. 20nM OA treatment demonstrates significantly higher pTau fluorescence. Kruskal-Wallis test, * *p = 0.042*

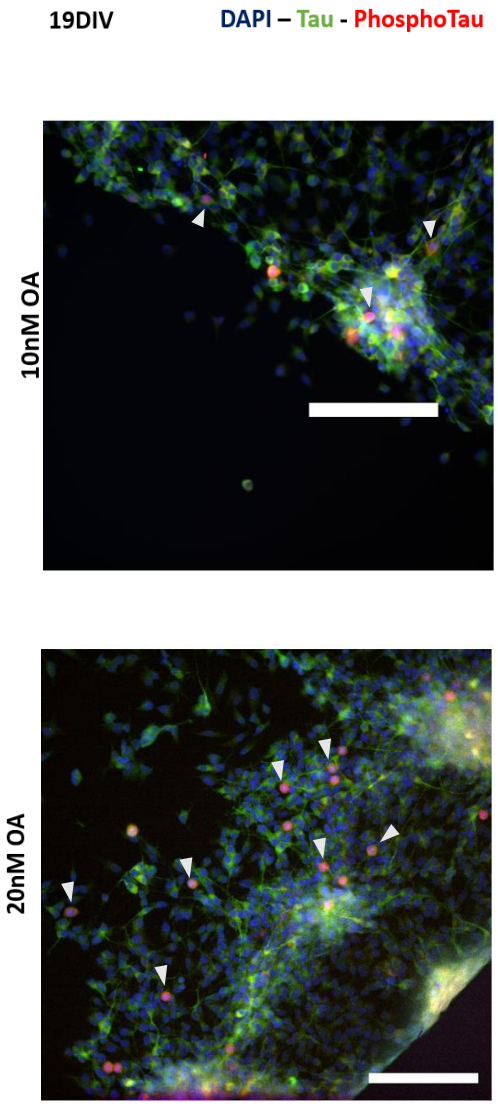

Figure 5 - Immunofluorescence images of 19 days in vitro SH-SY5Y cells treated with 10 or 20 nM okadaic acid for 2 hours. OA-treated SH-SY5Y cells demonstrate hyperphosphorylated Tau proteins located more towards the cell soma (pTau, red, arrowheads) rather than in the branches (Tau, green). Scale bar 175 µM.

SH-SY5Y cells express calcium signalling events.

To check the neuronal activity of our differentiated SH-SY5Y cells, calcium imaging was performed by the means of fluorescently analysing intracellular calcium levels. Cells were stained with Fluo-4 AM and treated with a calcium ionophore (ionomycin) as positive control. As seen in **figure 6**, stimulated SH-SY5Y cells exert higher levels of Fluo-4 AM, a cell-permeable fluorescent calcium indicator. No significant results are obtained yet. However, indications of intracellular calcium increases were obtained when differentiated SH-SY5Y cells were seeded on IBIDI 8-well glass inserts. Ionomycin stimulus was applied to increase intracellular calcium levels. Quantification of results was based on the total cell fluorescence, determined by the CTCF-formula (CTCF = Integrated Density – (Area of selected cell X Mean fluorescence of background readings). Higher calcium levels were obtained after stimulation (**Fig. 6 C**).

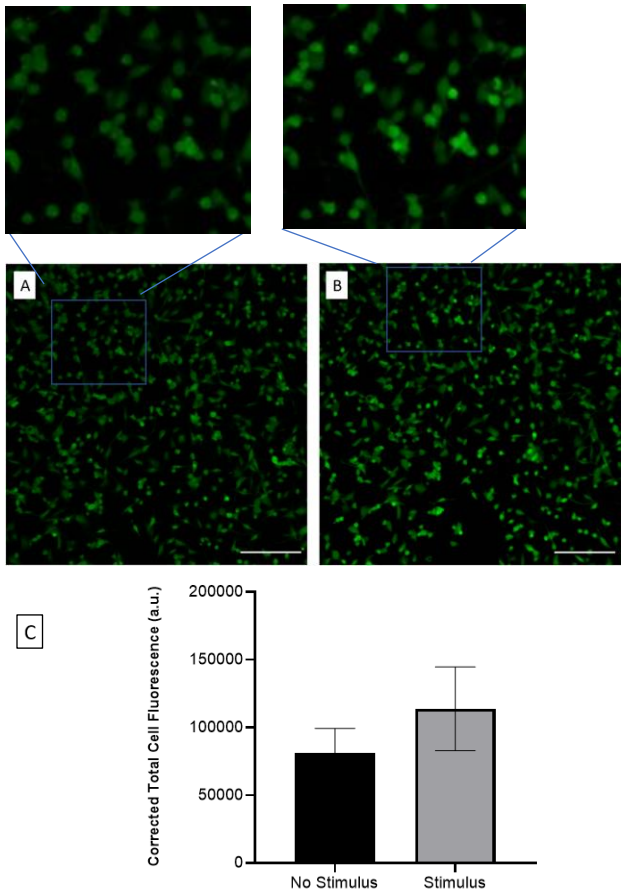

Figure 6 - Calcium imaging of (un)stimulated SH-SY5Y cells indicating intracellular calcium levels . SH-SY5Y cells were incubated at 37°C for 1 h with Fluo-4 AM containing buffer in the presence of probenecid. Images were taken before **(A)** and after stimulation with 10 µM ionomycin **(B)** with a fluorescence microscope using the FITC channel. Images were recorded every 5s for 61 seconds. **C)** The fluorescence images were quantified using ImageJ software and corrected total cell fluorescence was determined [by using following formula CTCF = Integrated Density – (Area of selected cell X Mean fluorescence of background readings)]. Scale bar 142 µm.

ROS induction in SH-SY5Y cells after H_2O_2 treatment as optimization before moving to induction of Aβ-pathology

Amongst the AD-related Tau pathology, we decided it is interesting to look at the other main pathological characteristic of AD, amyloid β plaques. Amyloid β fibrils are known to increase ROS production. Before fibril administration, we optimized the ROS assay by hydrogen peroxide treatment. We investigated the effects of H_2O_2 and the inhibitory effect of ascorbic acid, a ROS scavenger (32). To determine the ROS levels, a DCFDA assay was performed by measuring fluorescence values. All conditions were first measured at baseline and values at different time points were analyzed as fold change values. Treatment with 600 µM and 800 µM markedly increased the intracellular ROS levels in H_2O_2 treated SH-SY5Y cells (**Fig. 7)**. To verify protective effects of AA against H_2O_2-induced neurotoxicity in SH-SY5Y cells, cells were pretreated with increasing concentrations AA. Moreover, a ROS decreasing compound x, known to target the Aβ pathology, was taken into the experiments. Overall, pre-treatment with AA and compound x do show protective characteristics, suggesting that both protect the neuron-like SH-SY5Y cells against oxidative stress damage.

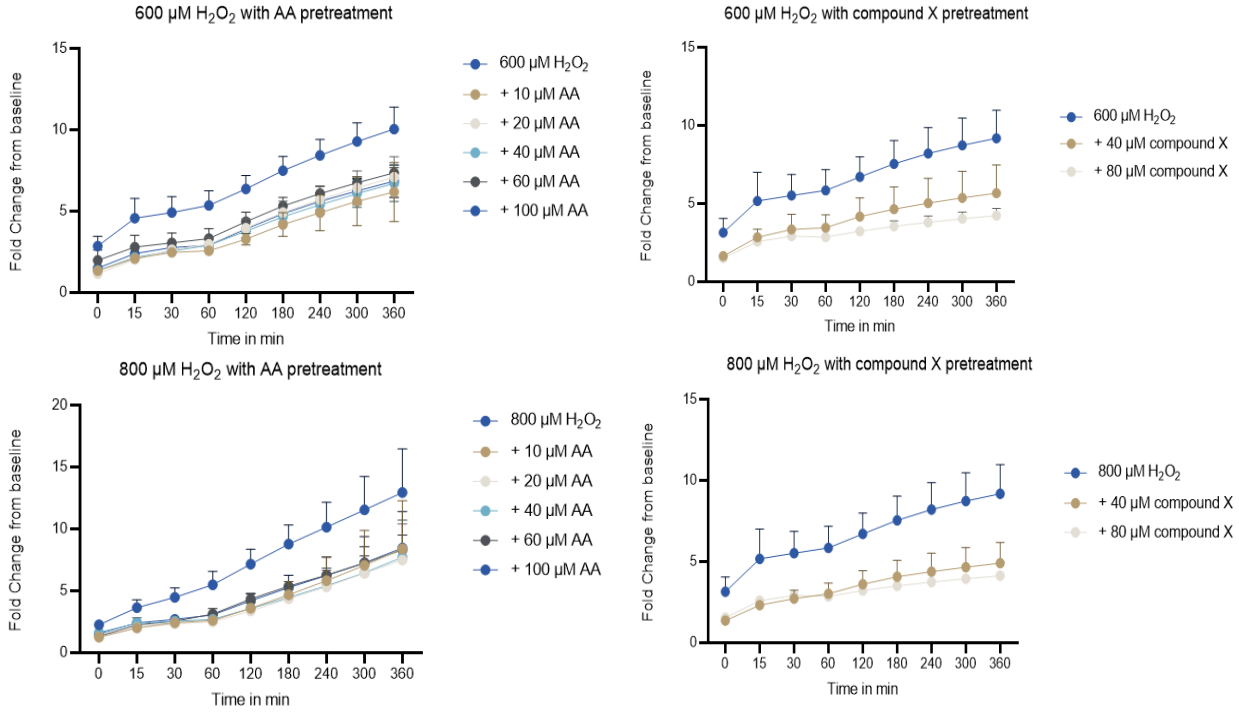

Figure 7 - Fold change values of ROS levels compared to baseline after H_2O_2 treatment with increasing concentrations of Ascorbic Acid (AA) and compound X pretreatment. Proof-of-concept experiment before Aβ-fibril induction. Cells were incubated with different concentrations H_2O_2 with time intervals; immediately after treating (0 min), 15 min, 30 min, 1 h, 2 h, 3 h, 4 h, 5 h and 6 h. Cells were pre-treated with a ROS scavenger (AA and compound X) to evaluate its effect on ROS production. Data are shown as mean ± SEM. (n = 3 samples per condition)

The 3D spheroids were visibly generated.

Ultimately, the optimal *in vitro* model we can get is a 3D model. Hence 3D models address the coherence of different processes that cannot be recapitulated by either the *in vivo* or 2D *in vitro* models, offering an opportunity to better understand the complexity and connectivity of the healthy and unhealthy human brain. Therefore, generating spheroids from SH-SY5Y cells is the first step. Afterwards, induction of AD phenotype in the spheroids can take place (e.g., okadaic acid) and further experiments can be performed (e.g. IF staining). As an initial step, spheroids are generated by culturing 3 x 10^6 SH-SY5Y cells in the AggreWell800 plates **(Fig. 8 A)**. The day after, these cells are aggregated and form a spheroid. These spheroids are then replated into ultra-low attachment plates to prevent them from binding to the polystyrene surface of the wells plate, this way obligating cell clustering and survival of the spheroids. Ideally, spheroids are plated one spheroid per well, to ensure replicable results are obtained per spheroid (avoiding multiple spheroids clustered together to form larger entities). In first attempt, this failed as the spheroids were small, fragile and were sticking together. Our results are proof-of-concept results needed before assuming it is even possible to generate spheroids ready for quantitative analysis. Generation of spheroids was successful (**Fig. 8 B)** and will provide a good spheroid model for following potential experiments. Replating, however, needs optimization (**Fig. 8 C)**.

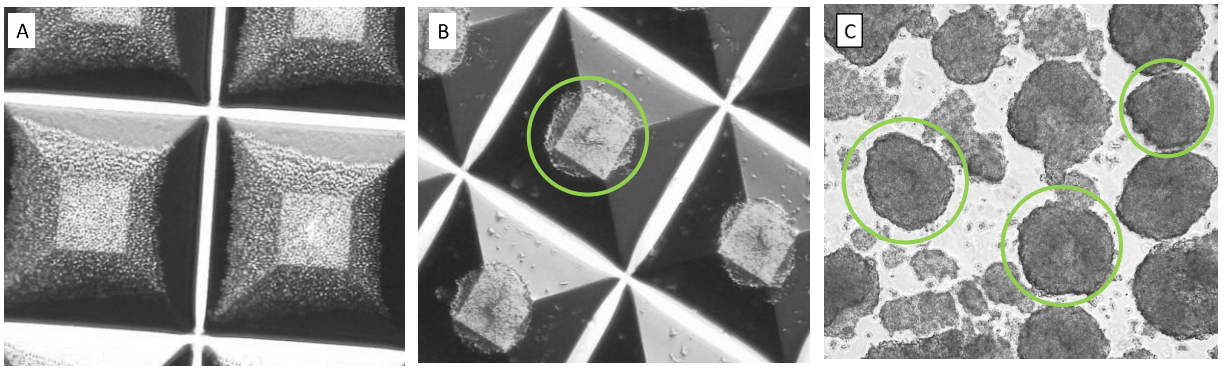

Figure 8 - Proof-of-concept gradual representation of spheroid generation in AggreWell™ 800. **A)** 3 x 10^6 SH-SY5Y cells are cultured in 1 well. **B)** The day after, these cells are attached to each other and form a spheroid. **C)** These spheroids are then replated into ultra-low attachment plates to provide them from sticking to the polystyrene surface of the wells plate, this way ensuring healthy survival of the spheroids. The goal is to be able to replate these spheroids 1 by 1. In first instance, this failed as the spheroids are small, fragile and sticking together.

DISCUSSION

In this manuscript, we confirmed that differentiation of SH-SY5Y cells into neuronal-like cells is plausible yet requires specific differentiation circumstances. We succeeded in obtaining a functional neuronal cell model. This cellular *in vitro* model will be the easier and less expensive alternative before moving to expensive and high-maintenance primary neurons or stem cell-derived *in vitro* models in neuroscientific research. Moreover, inducing AD-like hyperphosphorylated Tau into this cell model was a crucial step to approach our goal, creating a cellular AD model. More interestingly, inducing the extracellular amyloid plaques in the same model was planned to be initiated. This way, our model will be a complete and more representable *in vitro* model for AD-related drug screening. To be able to assess the neuronal activity of the differentiated SH-SY5Y cells, the intracellular calcium levels were analyzed by the means of calcium imaging. Lastly, spheroid generation was initiated yet not fully optimized.

The above-mentioned human neuroblastoma cell line is currently being used in many instances in the field of neuroscience as a functional model for human neurons. The reason we opted for them was because of their human origin, neuronal properties and ease of maintenance (33). Predominantly, for any *in vitro* neuronal system, cells are differentiated into neurons in order to obtain the most representable data of what possibly is occurring in neurons *in vivo* (34). Studies have shown important differences between differentiated and undifferentiated SH-SY5Y cells. When left undifferentiated, the cells rapidly proliferate and express very few and short projections. However, differentiated SH-SY5Y cells reduce proliferation rates and extend long, branched processes. Moreover, differentiated cells express markers of mature neurons and lack the expression of glial markers (34). Most prominently, three important steps in this differentiation process have been reported several times and been taken into consideration in this project. The addition of retinoic acid (RA) is one of the most used methods for induction of SH-SY5Y differentiation. RA is a vitamin-A derivative known to possess powerful properties that inhibit cell growth and promote cellular differentiation. In many other studies, RA is also administered at a concentration of 10 µM for a minimum of 3-5 days. It has also been reported that RA downregulates the mRNA and protein levels of the differentiation-inhibiting basic helix-loop-helix (Id) transcription factors, this means that differentiation is enhanced when influenced by RA. RA activates the PI3K/Akt signaling pathway, which is a requisite for neuroblastoma cell differentiation (35). Moreover, RA promotes cell survival and decreases susceptibility to neurotoxins. Amongst RA addition, serum removal to induce differentiation is an important step (30). Serum removal in the second differentiation step is proven to increase neurite length and branching and

stops the proliferation of the S phenotype, the epithelial-like cells, which increases the neuron-like differentiation. Gradually removing serum from SH-SY5Y cells increases neurite length and branching as well as increasing the proportion of cells expressing mature neuronal markers (MAP2) (36).
On top of that, addition of brain-derived neurotrophic factor (BDNF) has been shown to support differentiation and maintenance of the mature neuronal phenotype. According to *Kovalevich et al.*, the combination of BDNF with serum removal can prevent the replication of the S-type SH-SY5Y cells (epithelial-like phenotype) (29, 30). Otherwise, the epithelial phenotype of these cells (S-type) is known to overpopulate the cell culture. *Shipley et al.* reported that even the protocol of trypsinizing SH-SY5Y cells determines the proportion of N- or S-type cells. When trypsinization is performed in a short time interval, the loosening of only the N-subtype is ensured. The epithelial-like S-phenotype needs more time to detach (34).
Our data corroborate that RA induction and gradual serum removal in accordance with BDNF addition, contribute to correct differentiation of neuron-like cells. It has been reported that the continuous presence of serum in SH-SY5Y cultures, results in the S-type cells overgrowing the culture. As seen in **figure 1**, cells differentiating in DF1 (with RA and half reduction of serum) and later in DF2 (no serum at all, with BDNF) display a mature neuronal morphology, with rounder cell bodies and a robust network of neurites connecting them. Moreover, cells differentiated in BDNF-rich, serum-free medium visibly show a tendency to aggregate. In conclusion, the differentiation of SH-SY5Y cells to a neuron-like phenotype was a success.

Cells kept for 21DIV demonstrate a surprising dedifferentiation, cells lose their connectivity (determined as rate of neuronal branching) and viability (determined as equally spread living cells) as it is observable how some cells are formed into huge clusters while some reside one by one with lesser connections. On top of that, images taken of the 21DIV cell culture are not representable for neither neurite numbers nor visually demonstrating the condition of the culture as the culture contains both sparsely spread cells with strong neuronal branching towards each other yet also complex spheroid-like clusters of cells where neurites do not show up.

Interestingly SH-SY5Y cells are proven to be ideal cells for AD research. SH-SY5Y-derived neurons show expression of all six human brain Tau isoforms and a human brain-like Tau phosphorylation state (37). Moreover, *Bell et al.* highlighted the importance of differentiated SH-SY5Y cells in a Tau-related neurological model.

The induction of hyperphosphorylated Tau in our SH-SY5Y model, is the crucial step that will transform our simple neuronal model to the desired AD-NFT model. To do so, the neuron-like cells were treated with okadaic acid, a known protein phosphatase 2a inhibitor, leading to hyperphosphorylation of protein Tau. The cell viability results after 24 h OA treatment, at different concentrations, were considered to determine the treatment concentrations for immunofluorescence experiments. The 2h treatment with OA at these concentrations were considered to be likely resulting in abundant hyperphosphorylation of Tau compared to higher concentrations or longer duration of treatment, as these lead to cytotoxicity. The higher the OA treatment, the lower the chances of survival of the cells, as OA is known to be very toxic. Even though, OA treatments up to 50 nM were taken also into the IF experiments, no added value of these exist as the concentrations are already way too toxic. On the other hand, 20 nM does also show decreased viability after 24h treatment (**Fig. 3)** we still considered it possible for the immunofluorescence experiments. As expected, the 20 nM concentration showed the best staining results, both increasing pTau expression as still preserving cell viability. Consequently, okadaic acid-induced Tau hyperphosphorylation was succeeded. Cells demonstrated increased pTau fluorescence levels after OA treatment. On top of that, a clear distribution of pTau was seen in the cell soma, rather than the branches. In fact, this confirms the OA-induced AD-like Tau pathology. *Li et al.* demonstrated that phosphorylated Tau protein exhibits somatodendritic accumulation (38). Noticeably, cells at 14DIV seemed to not handle okadaic acid very well as neuronal branching was lacking after treatment and IF images were not as representable. Therefore, SH-SY5Y cells at 19DIV were also treated with OA and stained for Tau and pTau. As described before,

longer than 14DIV differentiation induces strong clusters of cells, yet this might be the reason better images were obtained at 19DIV, even after OA treatment. However, for the sake of individual cell analysis and validating the capacity of SH-SY5Y cells as AD model, quantitative analysis was still performed on 14DIV cells, again confirming the 20 nM treatment as optimal.
Although OA showed pTau induction and allows examination of effects on this process, this chemical induction method is still not ideal with respect to translational value. Induction of Tau hyperphosphorylation after amyloid fibril incubation will be examined as a next step based on the same readouts of cellular viability and pTau quantification (39).

Calcium imaging provides an indirect but accurate measure of action-potential generation within neurons. The rise in intracellular calcium during an action-potential triggers neurotransmitter release from the cell, causing cell-to-cell communication (40). SH-SY5Y human neuroblastoma cells are derived from human sympathetic neuronal tissue which makes them maintain many properties of nerve cells, including endogenously expressed voltage-gated calcium channels (41). Calcium imaging was performed to confirm neuronal activity in our differentiated neuroblastoma cell line. Calcium imaging, however, needs further optimization. No clear differences were observed between unstimulated and stimulated SH-SY5Y cells. Culture recipient materials might be a possible confounding factor and has been shown to be important for calcium assays. The initial experiments were performed in polystyrene plates, while glass plates have mainly been used in the literature (42). Different protocols and different culture materials were tested. Promising results were obtained with the Fluo4-AM protocol of Thermo Fisher Scientific and 8-well IBIDI glass insert. This was the only way to achieve visibly higher fluorescence in stimulated SH-SY5Y cells **(fig. 6 C)**. Unfortunately, no time was left to perform these experiments multiple times or to be able to analyse them more in detail. Therefore, validating this protocol is a planned priority. In addition, further optimization of imaging interval timeframes is needed. Future perspectives of this experiment are to optimize the imaging range and timing of SH-SY5Y cells, and opt for a better positive control than ionomycin. Ionomycin-induced calcium influx is known to induce neuronal degeneration, hence is not favourable as the cells will not be able to revive afterwards. Glutamate will be opted in further experiments as a positive control. This excitatory amino acid leads to a rise in the cytosolic free calcium concentration, thereby stimulating neuronal cells. Briefly, glutamate activates N-methyl-D-aspartate (NMDA) receptors, then calcium channels open resulting in an excess of intracellular calcium (43).
Obtaining calcium imaging is not only interesting to prove neuronal activity in our differentiated neuroblastoma cell lines but also because of the enrolment of calcium in AD, making it an interesting aspect of our model. *Cao et al.* reported that accumulation of intracellular calcium ions is responsible for the phosphorylation of Tau. Dysregulation in calcium homeostasis is also associated with cell exposure to Aβ and likely underlies its neurotoxic effects (44). Unsurprisingly, it was also reported by *Datta et al.* that neurons in the prefrontal cortex demonstrate a calcium leak with advancing age, which then in turn leads to the accumulation of phosphorylated Tau proteins causing the hallmark neurofibrillary tangles in the brain. Moreover, with age neurons tend to lose calbindin, which is a key regulator of calcium signalling protecting neurons from calcium overload (45). Thus, both an excessive amount of calcium and diminished levels of protectants contribute to the development of AD in elderly brains. The purpose of this manuscript was to develop a simple yet functional *in vitro* model for AD drug screening. Unfortunately, no standardized protocol for calcium imaging existed yet on-site.

We successfully analysed ROS levels in our SH-SY5Y models. This was purposedly optimized before moving towards creating a full AD model with the Aβ pathology included. To do so, we treated our cells with a ROS scavenger and hydrogen peroxide. *Zhao et al.* demonstrated the oxidative stress inducing effect of H_2O_2 on SH-SY5Y cells (46). More specifically, a ROS decreasing compound (referred to as compound x in this manuscript) created to target Aβ pathology in AD patients was planned to be analysed in our SH-SY5Y model. Literature suggested that ascorbic acid (AA), vitamin-C, is a well-known antioxidant scavenging free radicals and ROS (47,

48). Therefore, increasing concentrations of AA, known to decrease ROS levels, was taken into our experiments as a control to compound x (49). Our data confirmed ROS production and protection by both AA as compound x. Consequently, we obtained a functional ROS protocol and our model is ready to be treated with Aβ-fibril to analyse oxidative stress processes involved in AD and the effect of compound x on it.

As mentioned before, generating a functional 3D cellular model is the next step in our multi-step screening platform. *Seidel et al.* demonstrated it was possible to induce AD-like Tau pathology in the SH-SY5Y-derived neuronal 3D cell culture model. They validated high suitability of a 3D in vitro tauopathy cell model as a valid alternative to 2D cell models and complex animal models (50). Unfortunately, spheroid generation showed more hurdles than expected. This can be due to most importantly, the culturing conditions of SH-SY5Y cells. We generated our SH-SY5Y spheroids in expansion medium and only after the replating step a switch to differentiation medium is performed. Literature suggests to avoid differentiation of these cells to generate SH-SY5Y spheroids (showing Tau pathology) and therefore generate more organotypic-like spheroids, however these are then rather neuroblastoma spheroids instead of neuronal spheroids (50). This protocol needs more optimization by performing multiple trials with different culture conditions. Immunofluorescence analysis of the 3D model should claim its relevance, in comparison to the 2D model, by showing higher connectivity, higher expression and clear mis-localization of pTau in the okadaic acid treated model.

CONCLUSION

In general, SH-SY5Y cells are a good model for AD considering their human origin, neuronal phenotype, expansion potential and their ability to recapitulate AD-related aspects like NFTs.

In conclusion, we succeeded in differentiating SH-SY5Y cells into a neuronal phenotype and inducing AD-related Tau pathology. Moreover, we started the first steps of inducing AD-related ROS pathology. Generating a 3D model however still needs optimization. The number of days *in vitro* the cells need to stay before replating them as single spheroids is still to be elucidated. Once optimization is finalized, future experiments will consider comparisons between 2D and 3D read-outs, to confirm the value of the 3D model. Our SH-SY5Y model will serve as a cheaper and faster model before moving to more complex stem cell-derived models carrying specific mutations. This way, our model will be the first step in a multi-step drug-screening platform.

Acknowledgements – Author NÜ is grateful for getting a master senior internship position at the Neurology Research Department of InnoSer Belgium and acknowledges the MINDMAP group for her senior project. Research was funded by the grant from the EUROSTARS consortium (the European Commission and VLAIO). NÜ wants to sincerely thank YF for accepting the senior internship and providing access to all necessities. TvN and JB are specially thanked for guiding, helping, teaching, and ensuring a fun and experience full period. PV is thanked for providing access to lab material and his general help during brainstorms. SA and AvH are gratefully thanked for guiding and helping throughout the animal facility and the *in vivo* experience.

Author contributions – The MINDMAP consortium conceived and designed the research. TvN, JB and NÜ designed the current manuscript's research project and performed all experiments and data analysis. YF provided assistance and guidance. NÜ wrote the manuscript. All authors carefully edited the manuscript.

REFERENCES

1. Gitler AD, Dhillon P, Shorter J. Neurodegenerative disease: models, mechanisms, and a new hope. Dis Model Mech. 2017;10(5):499-502.
2. Organization WH. Dementia. 2021.
3. Medeiros R, Baglietto-Vargas D, LaFerla FM. The role of tau in Alzheimer's disease and related disorders. CNS Neurosci Ther. 2011;17(5):514-24.
4. Killin LO, Starr JM, Shiue IJ, Russ TC. Environmental risk factors for dementia: a systematic review. BMC Geriatr. 2016;16(1):175.
5. Collaborators GBDDF. Estimation of the global prevalence of dementia in 2019 and forecasted prevalence in 2050: an analysis for the Global Burden of Disease Study 2019. Lancet Public Health. 2022;7(2):e105-e25.
6. Kumar A. Alzheimer Disease. Alzheimer Disease. PubMed2021.
7. Frozza RL, Lourenco MV, De Felice FG. Challenges for Alzheimer's Disease Therapy: Insights from Novel Mechanisms Beyond Memory Defects. Front Neurosci. 2018;12:37.
8. Bekris LM, Yu CE, Bird TD, Tsuang DW. Genetics of Alzheimer disease. J Geriatr Psychiatry Neurol. 2010;23(4):213-27.
9. Tiwari S, Atluri V, Kaushik A, Yndart A, Nair M. Alzheimer's disease: pathogenesis, diagnostics, and therapeutics. Int J Nanomedicine. 2019;14:5541-54.
10. Breijyeh Z, Karaman R. Comprehensive Review on Alzheimer's Disease: Causes and Treatment. Molecules. 2020;25(24).
11. Avila J, Lucas JJ, Perez M, Hernandez F. Role of tau protein in both physiological and pathological conditions. Physiol Rev. 2004;84(2):361-84.
12. Ball KA, Phillips AH, Wemmer DE, Head-Gordon T. Differences in beta-strand populations of monomeric Abeta40 and Abeta42. Biophys J. 2013;104(12):2714-24.
13. Zhang X, Song W. The role of APP and BACE1 trafficking in APP processing and amyloid-beta generation. Alzheimers Res Ther. 2013;5(5):46.
14. Kadowaki H, Nishitoh H, Urano F, Sadamitsu C, Matsuzawa A, Takeda K, et al. Amyloid beta induces neuronal cell death through ROS-mediated ASK1 activation. Cell Death Differ. 2005;12(1):19-24.
15. Guglielmotto M, Giliberto L, Tamagno E, Tabaton M. Oxidative stress mediates the pathogenic effect of different Alzheimer's disease risk factors. Front Aging Neurosci. 2010;2:3.
16. Sadigh-Eteghad S, Sabermarouf B, Majdi A, Talebi M, Farhoudi M, Mahmoudi J. Amyloid-beta: a crucial factor in Alzheimer's disease. Med Princ Pract. 2015;24(1):1-10.
17. Nhan HS, Chiang K, Koo EH. The multifaceted nature of amyloid precursor protein and its proteolytic fragments: friends and foes. Acta Neuropathol. 2015;129(1):1-19.
18. Yiannopoulou KG, Papageorgiou SG. Current and Future Treatments in Alzheimer Disease: An Update. J Cent Nerv Syst Dis. 2020;12:1179573520907397.
19. Winslow BT, Onysko MK, Stob CM, Hazlewood KA. Treatment of Alzheimer disease. Am Fam Physician. 2011;83(12):1403-12.
20. Schachter AS, Davis KL. Alzheimer's disease. Dialogues Clin Neurosci. 2000;2(2):91-100.
21. Anderson RM, Hadjichrysanthou C, Evans S, Wong MM. Why do so many clinical trials of therapies for Alzheimer's disease fail? Lancet. 2017;390(10110):2327-9.
22. Drummond E, Wisniewski T. Alzheimer's disease: experimental models and reality. Acta Neuropathol. 2017;133(2):155-75.
23. Vitek MP, Araujo JA, Fossel M, Greenberg BD, Howell GR, Rizzo SJS, et al. Translational animal models for Alzheimer's disease: An Alzheimer's Association Business Consortium Think Tank. Alzheimers Dement (N Y). 2020;6(1):e12114.
24. Salari S, Bagheri M. In vivo, in vitro and pharmacologic models of Parkinson's disease. Physiol Res. 2019;68(1):17-24.
25. Kapalczynska M, Kolenda T, Przybyla W, Zajaczkowska M, Teresiak A, Filas V, et al. 2D and 3D cell cultures - a comparison of different types of cancer cell cultures. Arch Med Sci. 2018;14(4):910-9.
26. Jackson EL, Lu H. Three-dimensional models for studying development and disease: moving on from organisms to organs-on-a-chip and organoids. Integr Biol (Camb). 2016;8(6):672-83.
27. Kim J, Koo BK, Knoblich JA. Human organoids: model systems for human biology and medicine. Nat Rev Mol Cell Biol. 2020;21(10):571-84.

28. Agholme L, Lindstrom T, Kagedal K, Marcusson J, Hallbeck M. An in vitro model for neuroscience: differentiation of SH-SY5Y cells into cells with morphological and biochemical characteristics of mature neurons. J Alzheimers Dis. 2010;20(4):1069-82.
29. Encinas M, Iglesias M, Liu Y, Wang H, Muhaisen A, Cena V, et al. Sequential treatment of SH-SY5Y cells with retinoic acid and brain-derived neurotrophic factor gives rise to fully differentiated, neurotrophic factor-dependent, human neuron-like cells. J Neurochem. 2000;75(3):991-1003.
30. Kovalevich J, Langford D. Considerations for the use of SH-SY5Y neuroblastoma cells in neurobiology. Methods Mol Biol. 2013;1078:9-21.
31. Schuhmacher D, Sontag JM, Sontag E. Protein Phosphatase 2A: More Than a Passenger in the Regulation of Epithelial Cell-Cell Junctions. Front Cell Dev Biol. 2019;7:30.
32. Akram NA, Shafiq F, Ashraf M. Ascorbic Acid-A Potential Oxidant Scavenger and Its Role in Plant Development and Abiotic Stress Tolerance. Front Plant Sci. 2017;8:613.
33. Xicoy H, Wieringa B, Martens GJ. The SH-SY5Y cell line in Parkinson's disease research: a systematic review. Mol Neurodegener. 2017;12(1):10.
34. Shipley MM, Mangold CA, Szpara ML. Differentiation of the SH-SY5Y Human Neuroblastoma Cell Line. J Vis Exp. 2016(108):53193.
35. Lopez-Carballo G, Moreno L, Masia S, Perez P, Barettino D. Activation of the phosphatidylinositol 3-kinase/Akt signaling pathway by retinoic acid is required for neural differentiation of SH-SY5Y human neuroblastoma cells. J Biol Chem. 2002;277(28):25297-304.
36. Thomson AC, Schuhmann T, de Graaf TA, Sack AT, Rutten BPF, Kenis G. The Effects of Serum Removal on Gene Expression and Morphological Plasticity Markers in Differentiated SH-SY5Y Cells. Cell Mol Neurobiol. 2021.
37. Bell M, Zempel H. SH-SY5Y-derived neurons: a human neuronal model system for investigating TAU sorting and neuronal subtype-specific TAU vulnerability. Rev Neurosci. 2022;33(1):1-15.
38. Li C, Gotz J. Somatodendritic accumulation of Tau in Alzheimer's disease is promoted by Fyn-mediated local protein translation. EMBO J. 2017;36(21):3120-38.
39. De Felice FG, Wu D, Lambert MP, Fernandez SJ, Velasco PT, Lacor PN, et al. Alzheimer's disease-type neuronal tau hyperphosphorylation induced by A beta oligomers. Neurobiol Aging. 2008;29(9):1334-47.
40. Iosub R, Avitabile D, Grant L, Tsaneva-Atanasova K, Kennedy HJ. Calcium-Induced calcium release during action potential firing in developing inner hair cells. Biophys J. 2015;108(5):1003-12.
41. Sousa SR, Vetter I, Ragnarsson L, Lewis RJ. Expression and pharmacology of endogenous Cav channels in SH-SY5Y human neuroblastoma cells. PLoS One. 2013;8(3):e59293.
42. Barreto-Chang OL, Dolmetsch RE. Calcium imaging of cortical neurons using Fura-2 AM. J Vis Exp. 2009(23).
43. Wong RO. Effects of glutamate and its analogs on intracellular calcium levels in the developing retina. Vis Neurosci. 1995;12(5):907-17.
44. Cao LL, Guan PP, Liang YY, Huang XS, Wang P. Calcium Ions Stimulate the Hyperphosphorylation of Tau by Activating Microsomal Prostaglandin E Synthase 1. Front Aging Neurosci. 2019;11:108.
45. Datta D, Leslie SN, Wang M, Morozov YM, Yang S, Mentone S, et al. Age-related calcium dysregulation linked with tau pathology and impaired cognition in non-human primates. Alzheimers Dement. 2021;17(6):920-32.
46. Zhao X, Fang J, Li S, Gaur U, Xing X, Wang H, et al. Artemisinin Attenuated Hydrogen Peroxide (H2O2)-Induced Oxidative Injury in SH-SY5Y and Hippocampal Neurons via the Activation of AMPK Pathway. Int J Mol Sci. 2019;20(11).
47. Kawashima A, Sekizawa A, Koide K, Hasegawa J, Satoh K, Arakaki T, et al. Vitamin C Induces the Reduction of Oxidative Stress and Paradoxically Stimulates the Apoptotic Gene Expression in Extravillous Trophoblasts Derived From First-Trimester Tissue. Reprod Sci. 2015;22(7):783-90.
48. Yimcharoen M, Kittikunnathum S, Suknikorn C, Nak-On W, Yeethong P, Anthony TG, et al. Effects of ascorbic acid supplementation on oxidative stress markers in healthy women following a single bout of exercise. J Int Soc Sports Nutr. 2019;16(1):2.

49. Oh S, Kim YJ, Lee EK, Park SW, Yu HG. Antioxidative Effects of Ascorbic Acid and Astaxanthin on ARPE-19 Cells in an Oxidative Stress Model. Antioxidants (Basel). 2020;9(9).

50. Seidel D, Krinke D, Jahnke HG, Hirche A, Kloss D, Mack TG, et al. Induced tauopathy in a novel 3D-culture model mediates neurodegenerative processes: a real-time study on biochips. PLoS One. 2012;7(11):e49150.

SUPPLEMENTARY - Experimental Procedures

Table S1 – Used antibodies for immunofluorescence staining of differentiated SH-SY5Y cells.

Primary antibodies	Company	Cat. No.	Dilution	Species
Neurofilament 200	Sigma-Aldrich	N4142	1:300	Donkey-anti-Rabbit
Tau	ThermoFisher Scientific	13-6400	1:500	Donkey-anti-Mouse
pTau (Thr205)	ThermoFisher Scientific	44-738G	1:500	Donkey-anti-Rabbit
MAP2	Abcam	Ab92434	1:400	Donkey-anti-Chicken
Synaptophysin	Abcam	Ab32127	1:2500	Donkey-anti-Rabbit
PSD-95	Abcam	Ab13552	1:500	Donkey-anti-Mouse
Secondary antibodies	**Company**	**Cat. No.**	**Dilution**	**Species**
Alexa Fluor® 647	Abcam	Ab150075	1:500	Donkey-anti-Rabbit
FITC	Abcam	Ab63507	1:30	Donkey-anti-Chicken
Alexa Fluor® 555	Abcam	Ab150106	1:500	Donkey-anti-Mouse
NucBlue™ Fixed Cell ReadyProbes™ Reagent (DAPI)	ThermoFisher Scientific	R37605	2 drops/mL	Nuclear Dye

Table S2 – Medium compositions; SH-SY5Y culture.

SH-SY5Y Expansion Medium	Company	Cat. No.
Dulbecco's modified Eagle medium (DMEM)	Gibco	41966029
10% fetal bovine serum (FBS), heat inactivated	ThermoFisher Scientific	10438026
1% Penicillin/Streptomycin (P/S)	ThermoFisher Scientific	15070063
Differentiation Medium 1	**Company**	**Cat. No.**
DMEM, without pyruvate	Gibco	41965-039
5% FBS, heat inactivated	ThermoFisher Scientific	10438026
1% P/S	ThermoFisher Scientific	15070063
Retinoic Acid, 10 µM	Sigma	R2625
Differentiation Medium 2	**Company**	**Cat. No.**
Neurobasal-A medium minus phenol red	Gibco	12349015
L-Glutamine 2 mM	Gibco	25030024
N-2 Supplement	Gibco	17502048
Human brain-derived neurotrophic factor (BDNF), 50 ng/mL	Invitrogen	RP-8642
1% P/S	ThermoFisher Scientific	15070063

SUPPLEMENTARY - Results

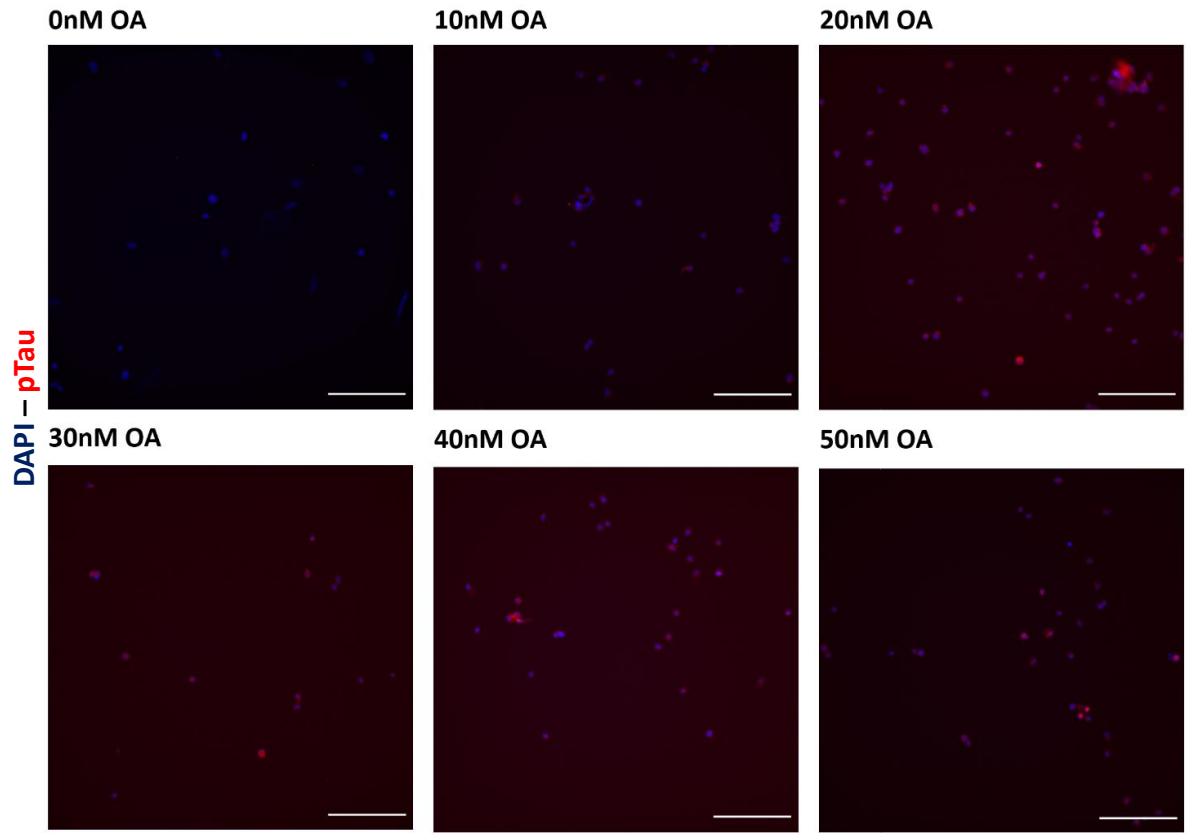

Supplementary figure 1 - Immunofluorescence images of 14 days in vitro SH-SY5Y cells treated with 0 nM, 10 nM, 20 nM, 30 nM, 40 nM and 50 nM okadaic acid for 2 hours. Okadaic acid treatment visibly induces pTau expression in all concentrations (except 0 nM). However, concentrations at 30 nM or higher visibly decrease the amount of living cells present in the culture, indicating a less favorable treatment for following experiments. Treating 14DIV SH-SY5Y cells with okadaic acid seems to be less representable than older neuron-like cells. Yet, 14DIV is the optimal "age" of single neuron-like cells and is taken into every experiment. Scale bar 150 µM.